Multimodal *In Vivo* Skin Imaging with Integrated Optical Coherence and Multiphoton Microscopy

Benedikt W. Graf, *Member, IEEE*, and Stephen A. Boppart, *Fellow, IEEE*

***Abstract*—In this paper, we demonstrate high-resolution, multimodal *in vivo* imaging of human skin using optical coherence (OCM) and multiphoton microscopy (MPM). These two modalities are integrated into a single instrument to enable simultaneous acquisition and coregistration. The system design and the OCM image processing architecture enable sufficient performance of both modalities for *in vivo* imaging of human skin. Examples of multimodal *in vivo* imaging are presented as well as time lapse imaging of blood flow in single capillary loops. By making use of multiple intrinsic contrast mechanisms this integrated technique improves the ability to noninvasively visualize living tissue. Integrated OCM and MPM has potential applications for *in vivo* diagnosis of various pathological skin conditions, such as skin cancer, as well as potential pharmaceutical and cosmetic research applications.**

***Index Terms*—*In vivo* imaging, multimodal microscopy, multiphoton microscopy (MPM), optical coherence tomography (OCT).**

I. Introduction

In RECENT years, various optical imaging modalities have emerged that enable high-resolution imaging of intact tissue. These modalities include reflectance confocal microscopy (RCM), multiphoton microscopy (MPM), and optical coherence tomography (OCT). One promising use of these techniques is for *in vivo* imaging of skin for both clinical and research applications. In dermatology, "optical sections" of live skin allows clinically relevant skin features to be noninvasively observed. This can be used to aid in the diagnosis of various skin diseases and minimize the need for invasive biopsy procedures. Commercial imaging systems for dermatology based on RCM [1], MPM [2] and OCT [3] are currently in use or undergoing clinical trials. In addition to clinical use, *in vivo* skin imaging has many research applications such as studying the effects of various cosmetic and pharmaceutical products [4], and assessing the development of engineered skin [5], [6]. The noninvasive nature of these imaging techniques enables repeated imaging of the same skin sites to observe dynamic events and long-term changes.

The various modalities used for *in vivo* skin imaging are based on different principles and enable various features of skin to be visualized. Reflectance confocal microscopy (RCM) provides subcellular resolution images of skin based on the optical scattering properties of a sample. Multiphoton microscopy (MPM) of skin also generates high-resolution images, but contrast is based on endogenous fluorescence properties as well as second harmonic generation (SHG) from collagen. MPM in combination with spectral or fluorescence lifetime detection is capable of distinguishing various endogenous fluorescent proteins in skin [7], [8]. Both RCM and MPM have sufficient spatial resolution to visualize single cells but both penetration depth and the field of view in skin are generally limited to several hundred micrometers. Optical coherence tomography (OCT) produces cross-sectional images of tissue structure based on the optical scattering properties. Conventional OCT has a penetration depth of roughly 1 mm in skin while the spatial resolution is typically 10–15 μm [4]. At this resolution skin appendages and blood vessels can be visualized. A high-resolution variation of OCT, called optical coherence microscopy (OCM), enables cellular level resolution, similar to RCM. However, in OCM, optical sectioning is achieved using coherence gating instead of spatial filtering, which has numerous advantages over RCM including greater sensitivity and deeper penetration [9].

While each of these imaging techniques has independently demonstrated its potential, the optimal instrument for *in vivo* skin imaging will likely be one that integrates multiple modalities. Multimodal imaging allows the strengths of different modalities to be simultaneously exploited. Using techniques based on different contrast mechanisms enables coregistration of distinct features or enhanced visualization of identical features. One particular combination of modalities that is promising for *in vivo* skin imaging, is OCM and MPM [10], [11]. The simultaneous use of these techniques provides high-resolution, multimodal contrast, and deep penetration in highly scattering tissue such as skin. MPM provides optical sections based on fluorescence while OCM provides 3-D scattering-based information. Integrated OCM-MPM has been used previously to monitor wound healing in skin-equivalent tissue models [12] and to perform optical biopsies of excised tissue samples [13]. Although OCM and MPM is a promising combination,

Manuscript received June 15, 2011; revised July 28, 2011; accepted August 14, 2011. The work was supported in part by the National Science Foundation (grants CBET 08-52658 ARRA, CBET 10-33906). The work of B. W. Grafs was also supported by the Predoctoral National Institute of Environmental Health Sciences Training Program in Endocrine, Developmental, and Reproductive Toxicology, the University of Illinois at Urbana-Champaign, IL.

This paper has supplementary downloadable material available at http://ieeexplore.ieee.org. This consists of three AVI format videos. They show, respectively, *en face* MPM images of *in vivo* human skin, *en face* OCM images of *in vivo* human skin, and time-lapse OCM imaging of a capillary. The size of this material is 11.9 MB.

B. W. Graf is with the Department of Electrical and Computer Engineering, University of Illinois at Urbana-Champaign, Urbana, IL 61801 USA (e-mail: bgraf@illinois.edu).

S. A. Boppart is with the Departments of Electrical and Computer Engineering, Bioengineering, and Internal Medicine, University of Illinois at Urbana-Champaign, Urbana, IL 61801 USA (e-mail: boppart@illinois.edu).

Color versions of one or more of the figures in this paper are available online at http://ieeexplore.ieee.org.

Digital Object Identifier 10.1109/JSTQE.2011.2166377

1077-260X/$26.00 © 2011 IEEE

integrating these modalities into a single system presents several technical challenges as they require different optical hardware to be performed optimally. Optimal performance of both modalities is crucial to make *in vivo* skin imaging feasible. Therefore, there is a need to develop methods for seamlessly integrating OCM and MPM into one instrument, while minimizing the loss of performance of either modality.

In this paper, we present multimodal *in vivo* imaging of human skin using an integrated OCM-MPM microscope. By simultaneously allowing sufficient performance of both modalities for *in vivo* imaging, this system increases the feasibility of this multimodal imaging technique. In the following section, we describe the challenges for combining OCM and MPM into one instrument and provide a detailed description of the microscope. This is followed by examples of high resolution, coregistered images from human skin *in vivo*. In addition, to enable imaging over a wide field of view, we demonstrate acquisition of wide area mosaics. Finally, we demonstrate dynamic imaging of blood flow in individual capillary loops. Integrated OCM and MPM enables *in vivo* multimodal visualization of skin based on intrinsic contrast and is a promising technique for clinical and research applications.

II. Materials and Methods

A. Tunable, Broad Bandwidth Laser Source

A primary challenge for combining OCM and MPM is that each modality requires a different type of laser source for optimal performance. The most common type of laser used for MPM is a wavelength-tunable Ti-sapphire laser with a relatively narrow optical bandwidth (10–20 nm) which allows a wide range of fluorescent markers to be targeted. OCM requires a laser source with a broad bandwidth (100–200 nm) to achieve an axial resolution of a few micrometers. To simultaneously meet these requirements, we utilize a previously developed dual spectrum laser source based on supercontinuum generation from a tunable Ti-sapphire laser [14]. The laser source for the integrated microscope is shown in Fig. 1(a). The linearly polarized output of the laser (Mai Tai HP, Spectra Physics) is split by a 90:10 beam splitter into two separate beams. The higher power beam is coupled into a photonic crystal fiber (LMA-PM-5, NKT Photonics) where through self-phase modulation the spectrum is broadened to 100–150 nm FWHM, depending on the center wavelength of the laser. The light from the fiber is collimated with an objective (20X Plan Apo NIR, Mitutoyo) and then directed to the OCM interferometer. The polarization maintaining fiber ensures that the OCM beam remains linearly polarized. The second portion of the laser beam is used directly for MPM imaging. A half wave plate is used to rotate the linear polarization of the MPM beam to make it orthogonal to the OCM beam. This allows the two beams to be recombined in the sample arm of the interferometer using a polarizing beam splitter. This laser source enables tuning of the wavelength to target a specific fluorescent marker for MPM while maintaining a broad spectral bandwidth for OCM, thus meeting the characteristics that each modality requires for optimal performance.

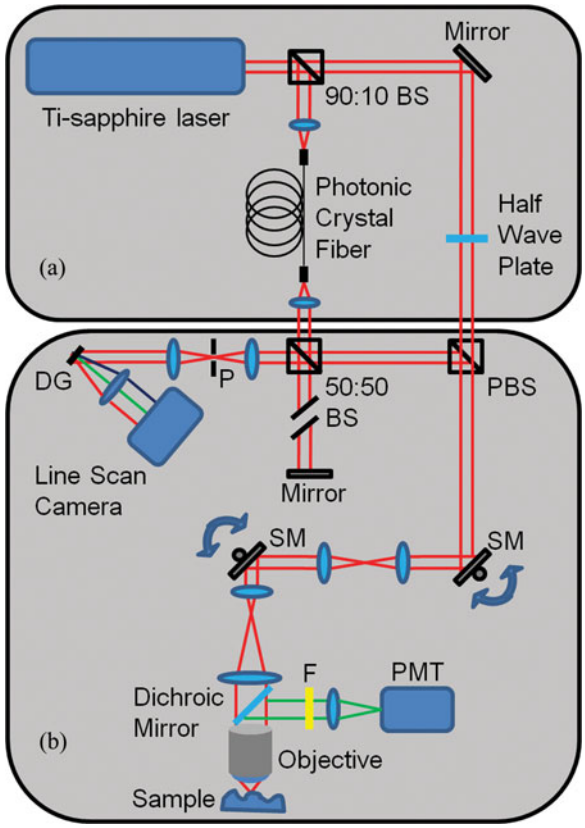

Fig. 1. Schematic of the integrated OCM and MPM system. The laser source (a) provides two separate beams to the OCM and MPM microscope (b), one for each modality. Abbreviations: BS, beam splitter; DG, diffraction grating; F, emission filter; P, pinhole; PBS; polarizing beam splitter; PMT; photo-multiplier tube; SM, scanning mirror.

B. Integrated OCM-MPM System Design

An additional challenge of combining OCM and MPM is that MPM requires the use of a very high numerical aperture (NA) objective lens (typically greater than 0.8). Such high NA is necessary to achieve high resolution and signal-to-noise ratio (SNR) for MPM, but effectively limits the depth-of-field for OCM to a single plane, similar to RCM. One of the primary advantages of OCM is that the axial resolution does not depend on NA, but instead on the coherence length. This decoupling of axial and transverse resolution in OCM allows imaging at cellular level resolution over a larger depth-of-field by using an intermediate NA of 0.4–0.6. In our system, the use of separate OCM and MPM beams allows the effective NA for each technique to be independently controlled while maintaining coregistration by using the same objective lens. By choosing optics to keep the size of the OCM beam smaller than the input aperture of the high NA objective lens, a lower NA for OCM is achieved. This allows OCM *en face* optical sections from multiple depths to be acquired simultaneously.

The schematic of the integrated OCM–MPM system is shown in part B of Fig. 1. The OCM beam is split into the reference and sample arms. In the sample arm, the OCM beam is recombined with the MPM beam using a polarizing beam splitter. The beam used for imaging thus contains a broadband component

and a narrowband component with orthogonal polarizations. The coincident beams are sent through a telecentric beam scanning assembly consisting of two galvanometers and a 1:1 telescope. The beam is then magnified by an additional telescope (1:3) before being focused onto the sample by a 0.95 NA objective (XLUMP20X, Olympus) with an input aperture of 18 mm. The $1/e^2$ beam diameter at the aperture is 16 mm for MPM and 10 mm for OCM, giving an effective NA of approximately 0.9 and 0.65, respectively. MPM signal generated at the focus is collected by the objective, deflected by a dichroic mirror and focused onto a PMT (H7421-40, Hamamatsu). An interchangeable filter detects the emission from the fluorescent marker of interest. The axial and transverse resolutions for MPM were experimentally determined by imaging fluorescent beads and were measured to be 0.8 μm and 0.5 μm, respectively. For OCM, backscattered laser light is recombined with the reference arm light in the interferometer and focused through a 15 μm pinhole using a 30 mm focal length achromatic lens. In this free space set up, the pinhole size determines the effective collection aperture for OCM. Considering the magnification due to the lenses between the pinhole and the sample, we calculate the collection aperture to be roughly 0.5 NA. The point spread function for OCM is determined by the product of the illumination and collection apertures [15]. The spatially filtered light is detected by a spectrometer consisting of a diffraction grating, focusing optics, and a line scan camera (Piranha2 2 k, Dalsa) with a maximum line rate of 32 kHz. The various hardware components are controlled and synchronized with a PC utilizing multiple data acquisition cards (National Instruments) and custom software written in LabVIEW.

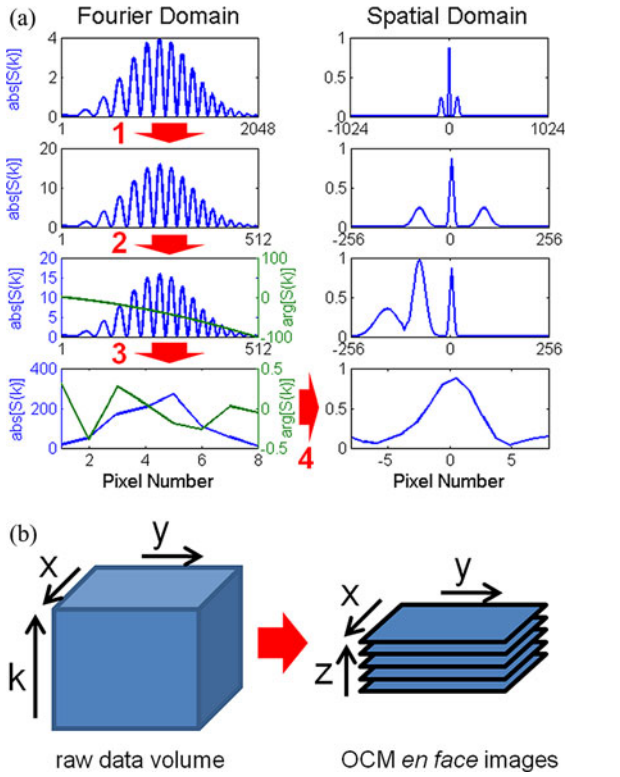

Fig. 2. Illustration of the image processing architecture for rapid reconstruction of OCM images. This architecture incorporates all the necessary preprocessing steps that are typical for OCT and reconstructs a short axial range using an FFT-zoom algorithm. (a) The processing steps for each spectral interference pattern showing the spectral and spatial domain at each step. The numbered red arrows indicate the actual processing steps executed (explained in detail in text). Each spectrum in the raw data volume is processed in this manner to reconstruct several *en face* OCM images, as illustrated in (b).

C. OCM Image Reconstruction

A critical factor that limits imaging speed is the computational demand of OCM. OCM requires multiple processing steps to reconstruct images, which can significantly impact the data acquisition speed. Necessary processing steps for each spectrum include imposing uniform spacing in wavenumber and numerical compensation of dispersion mismatch between the reference and sample arms [16]. In addition, the use of high NA optics and short coherence length results in curvature artifacts in the OCM images. This curvature is caused by optical path length changes in the sample arm that occurs with scanning of the beam. This effect results in a mismatch between the coherence gate and the confocal gate across the field of view and is referred to as coherence gate curvature [17]. The curvature must be compensated during image reconstruction in order to utilize the full field of view and enable coregistration with MPM images.

To overcome these challenges, we have developed an image processing architecture that enables high-speed reconstruction of OCM images. This approach, outlined in Fig. 2(a), corrects nonlinear spectral spacing, dispersion mismatch, coherence gate curvature, and allows multiple optical sections to be reconstructed in a computationally efficient manner. The first step in this process is to bin each 2048 pixel spectrum from the CCD by a factor of four [step 1 in Fig. 2(a)]. The size of the bin is varied across the spectrum such that the resulting spectrum is linear in wavenumber. Reducing the spectrum size also minimizes the computational cost of the remaining steps while maintaining necessary spectral resolution to reconstruct a depth range sufficient for OCM. In the second step of Fig. 2(a), each spectrum in the volume is multiplied by a unique phase profile that both corrects dispersion mismatch and computationally shifts the focal plane to the DC position in the spatial domain. The degree of spatial shift varies across the field of view of the OCM image thus correcting the curvature of the coherence gate. These phase profiles are obtained by calibrating the system using a mirror as the sample, as previously described [17]. Briefly, the Hilbert transform of each spectrum in the calibration data set is taken. This provides a phase profile consisting of a linear portion corresponding to the depth position of the mirror and higher order terms which are due to dispersion mismatch. Computationally shifting the focal plane to the DC position not only corrects the coherence gate curvature but also allows OCM images to be reconstructed using a fast Fourier transform zoom (FFT-zoom) algorithm. The third step in Fig. 2(a) consists of additional binning of each spectrum to a final size of 8 pixels as well as zero padding with an additional 8 pixels to double the spatial sampling. Decreasing the spectrum size limits the depth range in the spatial domain to the focal volume while zero padding increases the spatial sampling. Taking the FFT of this

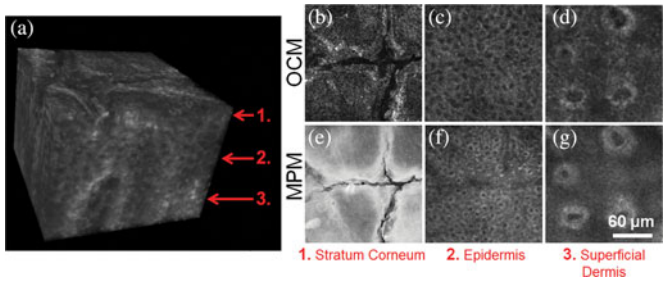

Fig. 3. High-resolution OCM and MPM images from *in vivo* human skin (see supplementary videos). A 3-D rendering of a merged OCM z-stack is shown (a) as well as *en face* OCM and MPM images from representative depths, (b–d) and (e–g), respectively. *En face* images are from the stratum corneum (b), (e), the epidermis (c), (f) and the superficial dermis (d), (g).

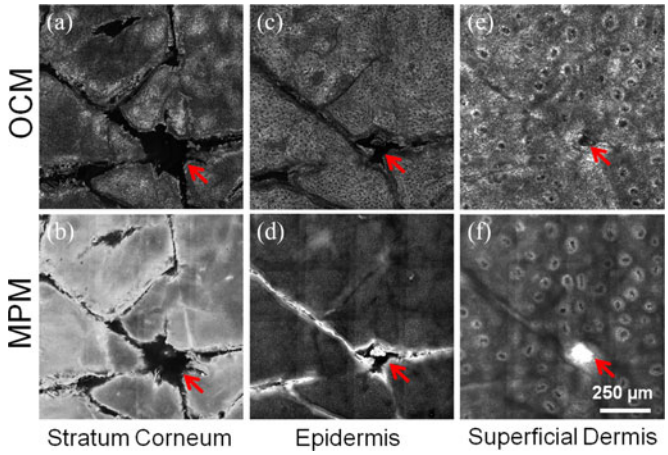

Fig. 4. Wide area OCM and MPM mosaics from *in vivo* human skin from three representative depths. Images are from the stratum corneum (a), (b), the epidermis (c), (d) and the superficial dermis (e), (f). Mosaics increase the field of view and allow larger skin features, such as hair follicles (indicated by red arrows), to be visualized.

spectrum reconstructs the axial scattering profile at 16 different depths within the focal volume at twice the spatial sampling [step 4 in Fig. 2(a)]. This process is repeated for each spectrum acquired at each beam position to reconstruct a 3-D volume, as illustrated in Fig. 2(b).

D. In Vivo Human Skin Imaging

To enable *in vivo* human skin imaging, an imaging mount was designed to keep the skin stabilized during image acquisition with the galvanometer-scanned mirrors. This mount consists of a thin glass coverslip mounted to a rigid holder. The skin is positioned against the coverslip during imaging to minimize motion artifacts. A small amount of glycerol is applied to the skin prior to imaging to serve as an index-matching agent. The imaging mount is attached to a motorized stage, which enables the focal depth to be adjusted in addition to allowing wide area mosaics to be acquired. Scanning the imaging mount over a range of several millimeters does not disturb the relative position of the skin to coverslip. To enable sufficient MPM excitation of the endogenous fluorescent proteins (primarily NADH and FAD [18]), the center wavelength of the laser was set to 760 nm. At this wavelength, the FWHM bandwidth of the laser is 10 nm while the generated supercontinuum has an FWHM bandwidth of 120 nm. The power level of the MPM beam at the sample was no greater than 15 mW, while the OCM beam was typically 5 mW. All imaging was done in accordance with protocols approved by the Institutional Review Board at the University of Illinois at Urbana-Champaign.

III. Results

A. High-Resolution Multimodal In Vivo Skin Imaging

To demonstrate high-resolution multimodal imaging, OCM-MPM images were simultaneously acquired at multiple focal positions from the dorsal hand of a human volunteer. Fig. 3 shows a 3-D rendering of merged OCM images from different focal depths in the skin, in addition to single OCM and MPM sections from three representative depths. In the OCM and MPM images from the top layer of the skin [Fig. 3(b) and (e), respectively], the stratum corneum, the microscopic surface topology is visible. In Fig. 3(c) and (f), acquired from the epidermis of the skin, single-cell nuclei from keratinocytes are visible. Deeper in the skin, dermal papillae are visible in both the OCM and MPM images [Fig. 3(d) and (g)]. Dermal papillae are the finger-like projections of the dermis into the epidermis and are part of the uneven junction between these two layers. This 3-D dataset consists of 50 *en face* planes (sections) taken with 3 μm focal steps in the axial (depth) direction, and 256 $\times$ 256 pixels in the lateral dimensions. For each focal position, 16 *en face* OCM images were reconstructed over a range of roughly 15 μm. Overlapping OCM images acquired from different focal positions were averaged to construct the 3-D OCM volume. Spatial dimensions are 230 $\times$ 230 $\times$ 150 μm for x, y, and z dimensions, respectively. Total acquisition time for this volume was 2.5 min.

B. Wide Area Mosaic

A primary limitation of high-resolution optical microscopy is that the fields of view are limited to several hundred micrometers. For many applications, it is desirable to survey larger areas of the skin than are possible with one image acquisition. The integrated microscope enables automated acquisition of wide-area mosaics of *in vivo* skin using a motorized stage. Fig. 4 shows several 4 $\times$4 OCM and MPM mosaics taken from different skin layers covering an area of approximately 1 $\times$ 1 mm. Larger features of the skin such as a hair follicle are visible in Fig. 4. Mosaicing allows the field-of-view to be increased arbitrarily while retaining high spatial resolution. Total acquisition time for each mosaic was less than 1 min.

C. Dynamic Imaging of Blood Flow in Capillaries

The high-speed capabilities of this microscope allow the dynamics of living skin to be visualized. With the high spatial resolution, it is possible to observe red blood cells moving through single capillaries. The dermal papillae in the skin contain capillary loops, which carry oxygen and nutrients to the upper regions of the epidermis. Time lapse OCM imaging of such a capillary

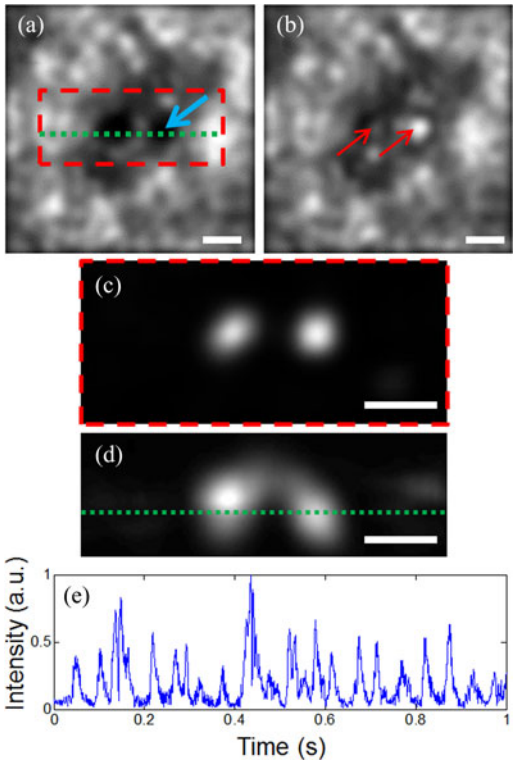

Fig. 5. Time lapse imaging of blood flow in a capillary loop in human skin (see supplementary video). (a) An *en face* OCM frame of a capillary loop in the absence of red blood cells clearly shows the ascending and descending capillary. (b) In a subsequent frame, red blood cells are present, giving a strong scattering signal from within the capillary [red arrows in (b)]. The change in scattering signal over time allows capillaries to be visualized at high contrast by displaying the variance of the time lapse OCM volumes. (c) *En face* and (d) cross-sectional slices from the time-variance volume shows the capillary loop. The orientation of the *en face* and cross-sectional variance images are indicated by the red dashed box and green dashed line in (a), respectively (scale bar is 15 μm). (e) Measurement of the scattering signal over time when the imaging beam is kept stationary at a capillary [blue arrow in (a)]. Peaks in the scattering signal are due to single cells passing through the capillary.

loop was performed to demonstrate the ability to visualize blood flow *in vivo*. Fig. 5(a) shows an *en face* OCM frame of a capillary loop within a dermal papillae in the absence of any red blood cells. The ascending and descending parts of the capillary loop are visible as the dark circular regions. In a subsequent frame [Fig. 5(b)] red blood cells (RBCs) are present in the capillary and result in a strong scattering signal. Time lapse OCM imaging results in rapid fluctuations in the backscattering signal from within the capillaries. These fluctuations can be utilized to visualize the capillaries by plotting the variance of the scattering signal over time from each spatial position in the 3-D OCM volume. This results in a 3-D image of the capillary loop. Fig. 5(c) and (d) show *en face* and cross-sectional slices of a capillary loop, respectively. The time-lapse data consisted of 50 OCM volumes taken at 3 s intervals. In addition to visualizing capillaries, it is possible to detect the movement of single cells moving through a capillary. Fig. 5(e) shows the scattering signal from one position in a capillary over a period of 1 s. The presence of an RBC in the capillary results in a spike in the scattering signal.

IV. Discussion

In this paper, we have presented multimodal *in vivo* imaging of human skin using an integrated OCM-MPM microscope that is designed to maximize performance for both modalities. Previous efforts to integrate these modalities into a single system have demonstrated the utility of coregistered OCM-MPM imaging for various applications but have not been used for *in vivo* imaging [10], [11], [19]. *In vivo* imaging presents many challenges as it requires high imaging speed and maximized signal-to-noise ratio. For OCM, imaging speed is limited largely by computational demands while MPM is limited in part by the low efficiency of auto fluorescence excitation. The integration of these modalities into a single system presents challenges due to the different optical hardware requirements of the two techniques. Despite these challenges, there is considerable benefit to this integrated approach for *in vivo* skin imaging for clinical and research applications.

The design of the integrated microscope and the OCM image processing architecture presented in this paper enables sufficient performance of both modalities for *in vivo* imaging of skin. An important aspect of the design is the dual spectrum laser source. Previously reported integrated OCM-MPM systems have largely relied on fixed wavelength, broadband Ti-Sapphire lasers for both MPM excitation and OCM imaging [10], [11], [19]. While this provides sufficient spectral bandwidth for OCM, it results in suboptimal MPM autofluorescence excitation in skin due to the strong wavelength dependence [18]. The dual spectrum source utilized on our system allows tuning of the center wavelength to provide efficient autofluorescence excitation at 760 nm while maintaining broad bandwidth for high resolution OCM imaging. An additional benefit of using separate beams for OCM and MPM is that the NA for each modality can be independently controlled. While very high NA ($>$0.8) is common for MPM, OCM typically utilizes a lower NA to allow a larger depth of field. While our current setup utilized a relatively large beam NA for OCM (0.65), it is possible to decrease this if a larger depth of field is required. In addition, a larger usable depth of field can be achieved by implementing interferometric synthetic aperture microscopy (ISAM) [20] to improve out of focus resolution or by utilizing an extended depth of focus method, such as an axicon lens [21].

The performance of an integrated OCM-MPM system is also limited by the high computational demand of OCM as well as coherence curvature effects caused by beam scanning in high NA systems [17]. Previously reported systems have avoided curvature effects by utilizing stage scanning for image acquisition [19], using common path interferometry [22] or by relying on confocal gating instead of coherence gating to limit the axial resolution [10]. However, these approaches either directly limit the ability to do *in vivo* imaging or reduce the performance of OCM. The method of OCM image processing presented in this paper computationally corrects coherence curvature artifacts and rapidly reconstructs OCM images from within the focal volume. By addressing some of the key limitations of OCM, this processing architecture facilitates the use of integrated OCM-MPM imaging for *in vivo* imaging of skin.

Despite the inherent challenges for simultaneous OCM and MPM imaging of *in vivo* skin, there is considerable benefit to this integrated approach. The combination of these modalities allows the use of both scattering and fluorescence-based contrast, which can provide complementary information about the condition of the skin. OCT/OCM [3] as well as RCM [1] have demonstrated the potential of scattering-based contrast for clinical applications. Based on the scattering intensity, macroscopic skin structure as well as microscopic features such as cell nuclei can be visualized. In addition, there are many variants of OCT/OCM that allow complementary features of the skin to be observed. These variants include polarization sensitive OCT for visualizing tissue birefringence due to collagen fibers [23], spectroscopic OCT for measuring wavelength dependent absorption [24] and for scatterer sizing [25] and various methods for visualizing vasculature based on phase sensitive measurements [26] or speckle variance [27]. MPM autofluorescence imaging has also independently demonstrated its clinical potential for skin imaging [2]. The fluorescence-based contrast enables both skin structure and single cells to be visualized. Combining MPM with spectral and fluorescence lifetime measurements has enabled various cell types in the skin to be distinguished [8] and also allows the rate of metabolism in cells to be measured [28]. The ability to simultaneously utilize scattering and fluorescence contrast with OCM and MPM thus has great potential to provide complementary information about the condition of skin. A recent clinical study has demonstrated the use of separate OCT and MPM instruments for imaging a variety of skin diseases and disorders [29]. The integrated OCM-MPM system presented in this paper enables inherent coregistration of the different modalities. Additional studies are needed to identify the best use of these different contrast mechanisms in order to maximize the clinical potential.

One of the most promising complementary variants of OCT/OCM is *in vivo* vasculature imaging. Various methods have been proposed based on the variance of time-lapse data [27] or by exploiting Doppler frequency shifts [26]. As vascular abnormalities are common with many skin diseases and conditions, vascular imaging has great potential for cancer diagnostics as well for studying skin diseases, such as psoriasis and port wine stains. In this paper, we utilize the high spatial resolution of OCM to visualize blood flow in a single capillary loop. Using the variance of the time-lapse data, we are able to visualize the capillary loop in three dimensions. Although MPM was not used in this case, the ability of OCM to visualize the skin vasculature based on intrinsic contrast is an additional benefit that can complement the MPM autofluorescence imaging. MPM imaging of blood vessels requires injection of fluorescent dyes into the blood stream, which is invasive and is thus less desirable for clinical applications. In addition to detecting blood vessels, it is possible to quantify the movement of single red blood cell by measuring the scattering signal from a fixed position over time. The combination of OCM and MPM has potential use for *in vivo* flow cytometry to detect fluorescently labeled circulating cancer cells [30], [31].

In conclusion, *in vivo* skin imaging with integrated OCM–MPM is a promising technique for clinical and research applications. The microscope used in this paper addresses the challenges of combining these modalities into a single system and increases the feasibility of this technique. Future work will utilize OCM–MPM to study the development and engraftment of engineered skin and for tracking fluorescently labeled bone-marrow derived stem cells in mouse skin *in vivo*. In addition, the integrated microscope will be used to visualize and track nanoparticles in *in vivo* mouse skin to study mechanisms of transport and biodistribution.

REFERENCES

[1] K. S. Nehal, D. Gareau, and M. Rajadhyaksha, "Skin imaging with reflectance confocal microscopy," *Semin. Cutan. Med. Surg.*, vol. 27, pp. 37–43, 2008.

[2] K. Konig and I. Riemann, "High-resolution multiphoton tomography of human skin with subcellular spatial resolution and picosecond time resolution," *J. Biomed. Opt.*, vol. 8, pp. 432–439, 2003.

[3] V. de Giorgi, M. Stante, D. Massi, L. Mavilia, P. Cappugi, and P. Carli, "Possible histopathologic correlates of dermoscopic features in pigmented melanocytic lesions identified by means of optical coherence tomography," *Exp. Dermatol.*, vol. 14, pp. 56–59, 2005.

[4] T. Gambichler, G. Moussa, M. Sand, D. Sand, P. Altmeyer, and K. Hoffmann, "Applications of optical coherence tomography in dermatology," *J. Dermatol. Sci.*, vol. 40, pp. 85–94, 2005.

[5] L. E. Smith, M. Bonesi, R. Smallwood, S. J. Matcher, and S. MacNeil, "Using swept-source optical coherence tomography to monitor the formation of neo-epidermis in tissue-engineered skin," *J. Tissue Eng. Regen. Med.*, vol. 4, pp. 652–658, 2010.

[6] W. Tan, A. Sendemir-Urkmez, L. J. Fahrner, R. Jamison, D. Leckband, and S. A. Boppart, "Structural and functional optical imaging of three-dimensional engineered tissue development," *Tissue Eng.*, vol. 10, pp. 1747–1756, 2004.

[7] J. A. Palero, H. S. de Bruijn, A. van der Ploeg-van den Heuvel, H. J. C. M. Sterenborg, and H. C. Gerritsen, "*In vivo* nonlinear spectral imaging in mouse skin," *Opt. Express*, vol. 14, pp. 4395–4402, 2006.

[8] E. Dimitrow, I. Riemann, A. Ehlers, M. J. Koehler, J. Norgauer, P. Elsner, K. Konig, and M. Kaatz, "Spectral fluorescence lifetime detection and selective melanin imaging by multiphoton laser tomography for melanoma diagnosis," *Exp. Dermatol.*, vol. 18, pp. 509–515, 2009.

[9] J. A. Izatt, M. R. Hee, G. M. Owen, E. A. Swanson, and J. G. Fujimoto, "Optical coherence microscopy in scattering media," *Opt. Lett.*, vol. 19, pp. 590–592, 1994.

[10] E. Beaurepaire, L. Moreaux, F. Amblard, and J. Mertz, "Combined scanning optical coherence and two-photon-excited fluorescence microscopy," *Opt. Lett.*, vol. 24, pp. 969–971, 1999.

[11] S. Tang, T. B. Krasieva, Z. Chen, and B. J. Tromberg, "Combined multiphoton microscopy and optical coherence tomography using a 12-fs broadband source," *J. Biomed. Opt.*, vol. 11, p. 020502, 2006.

[12] A. T. Yeh, B. S. Kao, W. G. Jung, Z. P. Chen, J. S. Nelson, and B. J. Tromberg, "Imaging wound healing using optical coherence tomography and multiphoton microscopy in an *in vitro* skin-equivalent tissue model," *J. Biomed. Opt.*, vol. 9, pp. 248–253, 2004.

[13] S. Yazdanfar, Y. Y. Chen, P. T. C. So, and L. H. Laiho, "Multifunctional imaging of endogenous contrast by simultaneous nonlinear and optical coherence microscopy of thick tissues," *Microsc. Res. Tech.*, vol. 70, pp. 628–633, 2007.

[14] B. W. Graf, Z. Jiang, H. Tu, and S. A. Boppart, "Dual-spectrum laser source based on fiber continuum generation for integrated optical coherence and multiphoton microscopy," *J. Biomed. Opt.*, vol. 14, p. 034019, 2009.

[15] B. J. Davis, S. C. Schlachter, D. L. Marks, T. S. Ralston, S. A. Boppart, and P. S. Carney, "Nonparaxial vector-field modeling of optical coherence tomography and interferometric synthetic aperture microscopy," *J. Opt. Soc. Am. a-Opt. Image Sci. Vision*, vol. 24, pp. 2527–2542, 2007.

[16] D. L. Marks, A. L. Oldenburg, J. J. Reynolds, and S. A. Boppart, "Digital algorithm for dispersion correction in optical coherence tomography for homogeneous and stratified media," *Appl. Opt.*, vol. 42, pp. 204–217, 2003.

[17] B. W. Graf, S. G. Adie, and S. A. Boppart, "Correction of coherence gate curvature in high numerical aperture optical coherence imaging," *Opt. Lett.*, vol. 35, pp. 3120–3122, 2010.

[18] H. G. Breunig, H. Studier, and K. Konig, "Multiphoton excitation characteristics of cellular fluorophores of human skin *in vivo*," *Opt. Express*, vol. 18, pp. 7857–7871, 2010.
[19] C. Vinegoni, T. Ralston, W. Tan, W. Luo, D. L. Marks, and S. A. Boppart, "Integrated structural and functional optical imaging combining spectral-domain optical coherence and multiphoton microscopy," *Appl. Phys. Lett.*, vol. 88, p. 053901, 2006.
[20] T. S. Ralston, D. L. Marks, P. S. Carney, and S. A. Boppart, "Interferometric synthetic aperture microscopy," *Nat. Phys.*, vol. 3, pp. 129–134, 2007.
[21] K. S. Lee and L. P. Rolland, "Bessel beam spectral-domain high-resolution optical coherence tomography with micro-optic axicon providing extended focusing range," *Opt. Lett.*, vol. 33, pp. 1696–1698, 2008.
[22] C. Joo, K. H. Kim, and J. F. de Boer, "Spectral-domain optical coherence phase and multiphoton microscopy," *Opt. Lett.*, vol. 32, pp. 623–625, 2007.
[23] M. J. Everett, K. Schoenenberger, B. W. Colston, and L. B. Da Silva, "Birefringence characterization of biological tissue by use of optical coherence tomography," *Opt. Lett.*, vol. 23, pp. 228–230, 1998.
[24] U. Morgner, W. Drexler, F. X. Kartner, X. D. Li, C. Pitris, E. P. Ippen, and J. G. Fujimoto, "Spectroscopic optical coherence tomography," *Opt. Lett.*, vol. 25, pp. 111–113, 2000.
[25] C. Y. Xu, C. Vinegoni, T. S. Ralston, W. Luo, W. Tan, and S. A. Boppart, "Spectroscopic spectral-domain optical coherence microscopy," *Opt. Lett.*, vol. 31, pp. 1079–1081, 2006.
[26] Z. H. Ding, Y. H. Zhao, H. W. Ren, J. S. Nelson, and Z. P. Chen, "Real-time phase-resolved optical coherence tomography and optical Doppler tomography," *Opt. Express*, vol. 10, pp. 236–245, 2002.
[27] A. Mariampillai, B. A. Standish, E. H. Moriyama, M. Khurana, N. R. Munce, M. K. K. Leung, J. Jiang, A. Cable, B. C. Wilson, I. A. Vitkin, and V. X. D. Yang, "Speckle variance detection of microvasculature using swept-source optical coherence tomography," *Opt. Lett.*, vol. 33, pp. 1530–1532, 2008.
[28] M. C. Skala, K. M. Riching, A. Gendron-Fitzpatrick, J. Eickhoff, K. W. Eliceiri, J. G. White, and N. Ramanujam, "*In vivo* multiphoton microscopy of NADH and FAD redox states, fluorescence lifetimes, and cellular morphology in precancerous epithelia," *Proc. Nat. Acad. Sci. U.S.A.*, vol. 104, pp. 19494–19499, 2007.
[29] K. Konig, M. Speicher, R. Buckle, J. Reckfort, G. McKenzie, J. Welzel, M. J. Koehler, P. Elsner, and M. Kaatz, "Clinical optical coherence tomography combined with multiphoton tomography of patients with skin diseases," *J. Biophotonics*, vol. 2, pp. 389–397, 2009.
[30] I. Georgakoudi, N. Solban, J. Novak, W. L. Rice, X. B. Wei, T. Hasan, and C. P. Lin, "*In vivo* flow cytometry: A new method for enumerating circulating cancer cells," *Cancer Res.*, vol. 64, pp. 5044–5047, 2004.
[31] Z. G. Fan, J. A. Spencer, Y. Lu, C. M. Pitsillides, G. Singh, P. Kim, S. H. Yun, V. Toxavidis, T. B. Strom, C. P. Lin, and M. Koulmanda, "*In vivo* tracking of 'color-coded' effector, natural and induced regulatory T cells in the allograft response," *Nat. Med.*, vol. 16, pp. 718–U125, 2010.

Benedikt W. Graf (M'09) was born in Red Bank, NJ, in 1985. He received the B.S. and M.S. degrees in electrical engineering from the University of Illinois at Urbana-Champaign, Urbana, IL, in 2007 and 2009, respectively, where he is working toward the Ph.D. degree in the Department of Electrical and Computer Engineering.

He was a Research Assistant in the Electro-Optics System Laboratory at the University of Illinois, from 2005 to 2007, and an Intern at HEP Prijenos, an electric power company in Croatia, in 2006. He is the recipient of a predoctoral fellowship from the NIEHS Training Program in Endocrine, Developmental and Reproductive Toxicology at the University of Illinois at Urbana-Champaign. He is a member of the Biophotonics Imaging Laboratory at Beckman Institute for Advanced Science and Technology. His research interests include the development of novel optical imaging techniques and image processing/analysis methods for clinical and research applications. Research applications include stem cell tracking in live skin and *in vivo* tracking of nanoparticles for studying mechanisms of transport and biodistribution.

Mr. Graf is a student member of the Optical Society of America. He received the E. C. Jordan Undergraduate Research Award from the University of Illinois, in 2007.

Stephen A. Boppart (S'90–M'90–SM'06–F'11) was born in Harvard, IL, in 1968. He received the B.S. degree in electrical and bioengineering and the M.S. degree in electrical engineering from the University of Illinois at Urbana-Champaign, Urbana, IL, in 1990 and 1991, respectively, the Ph.D. degree in electrical and medical engineering from the Massachusetts Institute of Technology, Cambridge, in 1998, and the M.D. degree from Harvard Medical School, Boston, MA, in 2000.

He was a Research Scientist with the Air Force Laser Laboratory, Brooks Air Force Base, San Antonio, TX, where he was engaged in research on developing national (ANSI) and Air Force laser safety standards. Since 2000, he has been with the University of Illinois at Urbana-Champaign, Urbana, from where he completed residency training in internal medicine in 2005. He is currently a Bliss Professor of Engineering in the Departments of Electrical and Computer Engineering, Bioengineering, and Medicine, and the Head of the Biophotonics Imaging Laboratory, Beckman Institute for Advanced Science and Technology, University of Illinois at Urbana-Champaign, and also the Director of the Illinois Imaging Initiative. He has authored or coauthored more than 205 invited and contributed publications, and more than 470 invited and contributed presentations. He holds more than 30 patents, filed or pending. His research interests include the development of novel optical imaging technologies for biological and medical applications, with particular emphasis on translating these to clinical applications in cancer detection and diagnosis.

Dr. Boppart is a Fellow of the Optical Society of America, and the International Society for Optical Engineering. He is a member of the Society for Molecular Imaging, the Academy of Molecular Imaging, the American Association for the Advancement of Science, the American Association for Cancer Research, and the American Medical Association. He was named one of the top 100 innovators in the world by the *Technology Review Magazine* for his research in medical technology in 2002. He received the IEEE Engineering in Medicine and Biology Society Early Career Achievement Award in 2005, and was recognized in 2009 with the Paul F. Forman Engineering Excellence Award from the Optical Society of America for dedication and advancement in undergraduate research education.